Materials and Design 142 (2018) 229–239

Contents lists available at ScienceDirect

Materials and Design

journal homepage: www.elsevier.com/locate/matdes

Design and fabrication of a non-clogging scaffold composed of semi-permeable membrane

Shiyi Tan, Jiafei Gu, Seung Chul Han, Dong-Weon Lee, Kiju Kang *

School of Mechanical Engineering, Chonnam National University, Gwangju 61186, Republic of Korea

HIGHLIGHTS

- A 3D polymer membrane architecture was proposed as a novel concept of bio scaffold.
- It had two sub-volumes that were intertwined but separated by a semi-permeable membrane.
- One sub-volume was used for cell culture, while the other served as a perfusion channel.
- Mass transfer was implemented through the interfacial semi-permeable membrane.
- Despite very high porosity, its strength & modulus was appropriate for bones or cartilages.

GRAPHICAL ABSTRACT

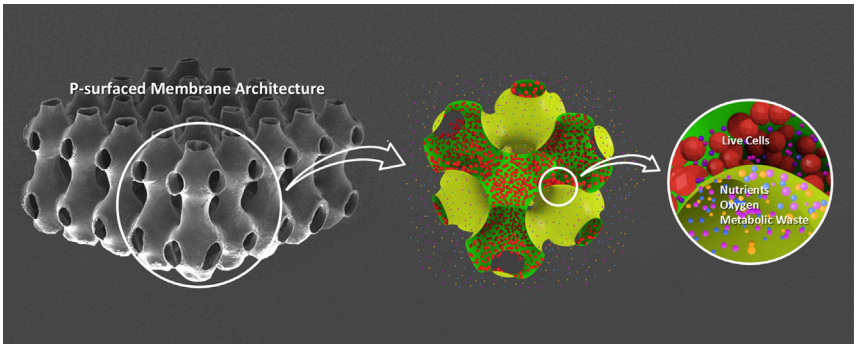

ARTICLE INFO

Article history:
Received 30 October 2017
Received in revised form 17 January 2018
Accepted 17 January 2018
Available online 3 February 2018

Keywords:
3D membrane architecture
Minimal surface
Scaffold
3D lithography

ABSTRACT

In this study, a novel concept of polymer scaffold was proposed based on 3D porous membrane architecture. It had two distinct sub-volumes intertwined with each other but separated by a single continuous smooth semi-permeable membrane. One sub-volume was used for cell culture, while the other served as a perfusion channel. Mass transfer was implemented through the interfacial porous membrane. Consequently, this scaffold was expected to be completely free from clogging problem due to growing tissue. The sample scaffolds of poly L-lactic acid (PLLA) was fabricated based on 3D UV photo-lithography and porogen leaching technique, which provided a P-surface-like architecture composed of porous membrane having smooth and fine texture with considerably high porosity. Despite high overall porosity of approximately 97%, these scaffolds had strengths and Young's moduli appropriate for regeneration of bones or cartilages. Wettability and permeability of polydopamine-coated PLLA porous membrane were sufficiently high.

1. Introduction

Tissue engineering is a multidisciplinary field that regenerates biological alternatives for damaged tissues and organs using a combination of cells, scaffolds, and bio-signals [1]. As an essential part of tissue engineering, the scaffold (i.e., artificial extracellular matrix) plays a crucial role in cell growth, proliferation, and new tissue regeneration in three dimensions. A variety of bioactive degradable scaffolds have been fabricated by various techniques such as particulate leaching, gas forming, freeze-drying and rapid prototyping in the past decades [2].

However, mass transfer limitation remains a serious challenge in the field of tissue engineering. In in-vitro engineering of living tissues, non-homogeneous growth of cells inevitably occurs in conventional porous solid scaffolds due to limitation in continuous delivery of nutrients and oxygen as well as limitation in removing metabolic waste products

* Corresponding author.
E-mail address: kjkang@chonnam.ac.kr (K. Kang).

https://doi.org/10.1016/j.matdes.2018.01.033
0264-1275/

[3]. Because the mass transfer is limited by growing cells, active cells that migrate into the deeper part of a porous structure can become necrotic. Almost no cells can survive far from the outer surface of more than 500 μm [3,4]. In conventional 3D structures such as salt-leached scaffolds, cells commonly congregate only at the outermost region.

Recently, porous materials with triply periodic minimal surface (TPMS) configuration have attracted attention as scaffolds for tissue engineering applications, because TPMS has zero (or "a constant" in a wider sense) mean curvature over the entire surface while being periodic in three directions [5]. TPMS partitions space into two disjointed but intertwined sub-volumes that are simultaneously continuous. To date, a scaffold in TPMS configuration comprises one solid sub-volume and another sub-volume of air (void), while the interface has TPMS configuration [6–11]. Because TPMS possesses desirable characteristics such as smooth surface, high surface area, excellent permeability, and sufficient mechanical strength and stiffness, a scaffold with TPMS is regarded as ideal for cell adhesion, migration, and vitalization in tissue engineering. The excellent permeability of such scaffold allows superior diffusion, facilitating the inflow of nutrients and disposal of metabolic waste, which can partly relieve clogging issues due to cell growth in perfusion channels (i.e., the void sub-volume). This type of scaffold has gained popularity because it can be precisely fabricated by means of CAD modeling and additive engineering [12,13].

Nevertheless, previous TPMS scaffolds are not free from clogging issues, because an identical place (i.e., the void sub-volume) is shared for dual functions of cell culture and perfusion. Consequently, penetration of cell culture is inevitably limited. In addition, the solid sub-volume is likely to be too dense as a scaffold for most applications in tissue engineering except for bone regeneration. The large portion of such solid sub-volume may be a burden for in-vivo degradation. Thus, higher porosity (i.e., lower relative density) is desirable.

A more recent approach is to use a cell-laden hydrogel reinforced with microfibers [14] or synthetic biomaterial [15–18]. Namely, the reinforced hydrogel is printed into a 3D lattice architecture and the interconnected interior pores function as perfusion channels. Because the cells are cultured in the hydrogel-based substance, while the pores are used for perfusion channels, this approach looks quite effective to solve the clogging issue, mentioned above. However, this approach may not be appropriate for regenerations of hard organs such as bone or cartilage.

Another effective approach to address the pervasive issue is to functionalize the scaffold by integrating perfusion channels that act as an artificial vascular system, enhancing mass transfer for cell growth [19]. Modified scaffolds designed with perfusion channels and fabricated by rapid prototyping [6] or lattice scaffolds combined with hollow fiber membranes [20] have significantly contributed to uniform distribution of cells. We regard the latter as the more effective way. Namely, the hollow fiber membranes act as perfusion channels of an artificial vascular system, while the lattice structure provides 3D spaces where the cells grow and proliferate and new tissues are regenerated. Mass transfer between cells and the perfusion channel, i.e., the inflow of oxygen and nutrients and disposal of metabolic waste, was implemented through the semi-permeable membranes of the hollow fibers.

Han et al. [21] have introduced a new type of 3D membrane architecture, named Shellular that is composed of a single continuous smooth membrane. In the authors' research group, it has been validated that a uniformly smooth surface results in high strength and stiffness; thereby TPMS is a good choice as the membrane architecture of Shellular [22–24]. Because TPMS has a smooth surface with a constant mean curvature, a Shellular in a TPMS configuration does not have stress concentration due to its geometrical irregularity, and it is likely to support external load by coplanar stresses, without causing bending stress. The thin membrane architecture of Shellular in TPMS configuration may serve as a stretching-dominated structure, as observed in trussed cellular materials, generally referred to as micro-architectured materials [25]. Also, as a 3D membrane architecture which supports internal pressure, Femmer et al. [26] showed effectiveness of TPMS configurations. In addition, it is expected that the thin continuous membrane in TPMS might play a role as transfer interface between two void sub-volumes as well as mechanical load support.

This study introduced a radical design of 3D membrane architecture as a novel functionalized tissue engineering scaffold. The conceptual model of this scaffold is shown in the upper of Fig. 1. Actually, this design is a combination of the above-mentioned two types of scaffolds: the scaffold in TPMS configuration with one solid sub-volume and the scaffold integrated with perfusion channels. This was composed of a semi-permeable polymer membrane in a form of TPMS Shellular with two non-intersecting void sub-volumes, as illustrated in the lower of Fig. 1. One sub-volume was used for cell culture, while the other served as a perfusion channel. Mass transfer between cells and the perfusion channel was implemented through interfacial semipermeable membrane. Namely, this intriguing scaffold was integrated with a vascular system (i.e., mass transfer channel); thereby it continuously provided nutrients and oxygen supply to proliferating cells as well as removal of waste through the thin semi-permeable membrane. Despite its ultra-lightness, this 3D membrane scaffold is expected to have sufficient strength needed for most organs, as mentioned above. Therefore, this scaffold plays dual roles as hollow fiber membranes and the lattice structure of Bettahalli's scaffold, mentioned above [20]. Each sub-volume of this scaffold in a TPMS Shellular has biomorphic geometry, which is ideal for facilitating cellular attachment and realizing uniform cell culture [7]. After the scaffold accomplishes its role of cell support and pseudo-vascularization, the 3D membrane architecture can be degraded and absorbed without causing any harm due to the small amount of solid material (i.e., the membrane). As a result of a preliminary study of such scaffold, this study described the fabrication process of the 3D membrane architecture developed for this purpose. Also, its mechanical properties, microstructure, wettability, and permeability were evaluated.

2. Materials and methods

2.1. Design of 3D membrane architecture

Among various TPMSs, *P*-surface was chosen as the 3D membrane architecture. *P*-Surface located in a cube of the unit cell size, D [7] is given by

$$\left(\cos\left(\frac{2\pi x}{D}\right)+\cos\left(\frac{2\pi y}{D}\right)+\cos\left(\frac{2\pi z}{D}\right)\right)+k_1=0, \tag{1}$$

where $x, y, z \in [-\frac{D}{2}, \frac{D}{2}]$, and k_1 is a level set value that decides the volume fraction, f, which is defined as ratio of the inner sub-volume to overall volume [7]. Calculation using a CAD program yielded relation between k_1 and f, and relation between surface area, A, and f as follows;

$$f = 0.29k_1 + 0.5 \quad \text{and} \tag{2}$$

$$\frac{A}{D^2} = -13.054(f-0.5)^4 - 4.555(f-0.5)^2 + 2.34, \quad \text{respectively.} \tag{3}$$

Eq. (3) reveals that surface area is the largest at $f = 0.5$. Because the 3D membrane architecture in this study was fabricated based on the technique, described in Han, et al. [21], geometry was elongated by a factor of k_2 in z-direction. Hence, the surface is given as follows:

$$\left(\cos\left(\frac{2\pi x}{D}\right)+\cos\left(\frac{2\pi y}{D}\right)+\cos\left(\frac{2\pi z}{k_2 D}\right)\right)+k_1=0 \tag{4}$$

Nevertheless, the surface area is still the largest at $f = 0.5$.

The authors chose the cell size of $D = 1$ mm, which may be appropriate for a scaffold for chondrocyte cells [27].

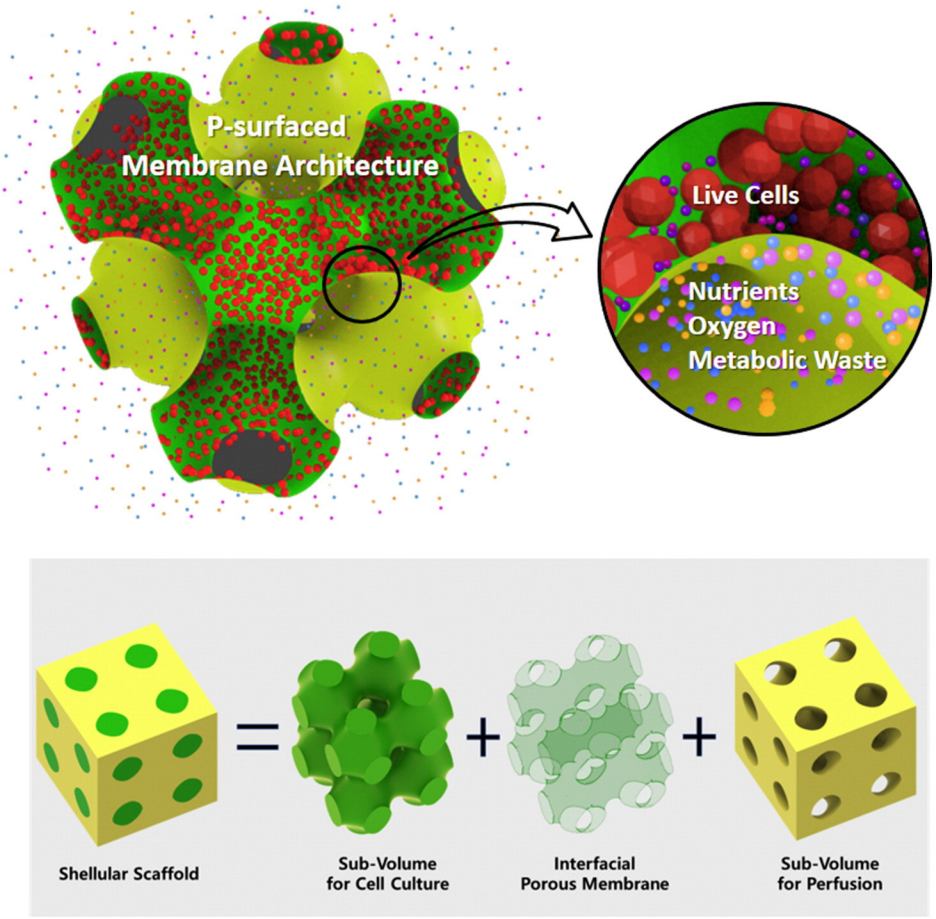

Fig. 1. A conceptual model of scaffold of a single continuous porous membrane of *P*-surface (top) and its composition with a semi-permeable polymer membrane between two non-intersecting void sub-volumes (bottom).

2.2. Specimen preparation

2.2.1. Materials

Poly L-lactic acid (PLLA) with molecular weight (MW) of 230 kDa was purchased from PolySciTech® (West Lafayette, IN, USA). It was the main constituent material of the 3D membrane architecture. Polyinyl alcohol (PVA), tris (hydroxymethy) aminomethane (Tris-HCl), dopamine hydrochloride (DA), phosphate buffered saline (PBS), and bovine serum albumin (BSA) were acquired from Sigma-Aldrich (St. Louis, MO, USA). Hot mounting resin (HMR: Model JZXM0241) was purchased from XinHui (Changsha) Electronic Technological Co. (Hunan, China). Polyethylene glycol (PEG) with average MW of 400, chloroform, 1,4-dioxane, and other reagents were acquired in reagent grade from Duksan Pure Chemical (Korea).

Fig. 2 shows the process used to fabricate specimens of the 3D membrane architecture. The process was divided into three steps: template formation, membrane material coating, and porous shell formation. Technical details are described in the following sections.

2.2.2. Template formation

First, a negative template was formed within a pool of photo-monomer thiol-ene, using self-propagating polymer waveguide (SPPW) [28]. UV exposure system used for forming the negative template is shown in Fig. 3A. Technical details are given in Han et al. [21]. Residual resin was washed out using toluene. The template was then heat-treated at 120 °C for 12 h to fully harden.

Powder of hot mounting resin (HMR) was poured over the negative template followed by heating to 150 °C to melt and fill the void of the negative template. After cooling, the outer surface of HMR was polished to expose the interior thiol-ene negative template, which was then etched in 4 wt% NaOH solution to obtain HMR positive template. To prevent the HMR template from damage due to organic solvent during subsequent multiple coatings of biopolymer, a protective layer of PVA was coated on the surface of the template by dip-spin coating with 15 wt% PVA water/ethanol (1:1) solution. Samples of the negative (top) and positive (bottom) templates with close-up top views are shown in Fig. 3B.

2.2.3. Membrane material coating

To obtain porous membrane, porogen leaching technique [29] was used. For this purpose, three different types of biopolymer coating solutions (Table 1) were prepared and tested to choose the proper one for fabricating the 3D membrane architecture. The details are as follows. For Type-I, PLLA and PEG with weight ratio of 1:1 were co-dissolved at a concentration of 12% wt/vol in chloroform by stirring with a magnetic stirring bar until the solution became transparent. For Type-II, PLLA and PEG with weight ratio of 1:1 were dissolved at a concentration of 12% wt/vol in blended solvent of chloroform and 1,4-dioxane with a volume ratio of 1:1. For Type-III, PLLA and PEG with weight ratio of 2:1 were dissolved at a concentration of 12% wt/vol in blended solvent of chloroform and 1,4-dioxane with a volume ratio of 1:1.

The template was dipped into one of the biopolymer coating solutions. It was then placed in a centrifuge for several seconds to remove the excess coating solution. The coated template was dried for 4–5 h at ambient condition with relative humidity of approximately 60%. The template coated with the biopolymer solution was heat-treated in an oven at 70 °C for 2 h to improve crystallinity of the coated layer.

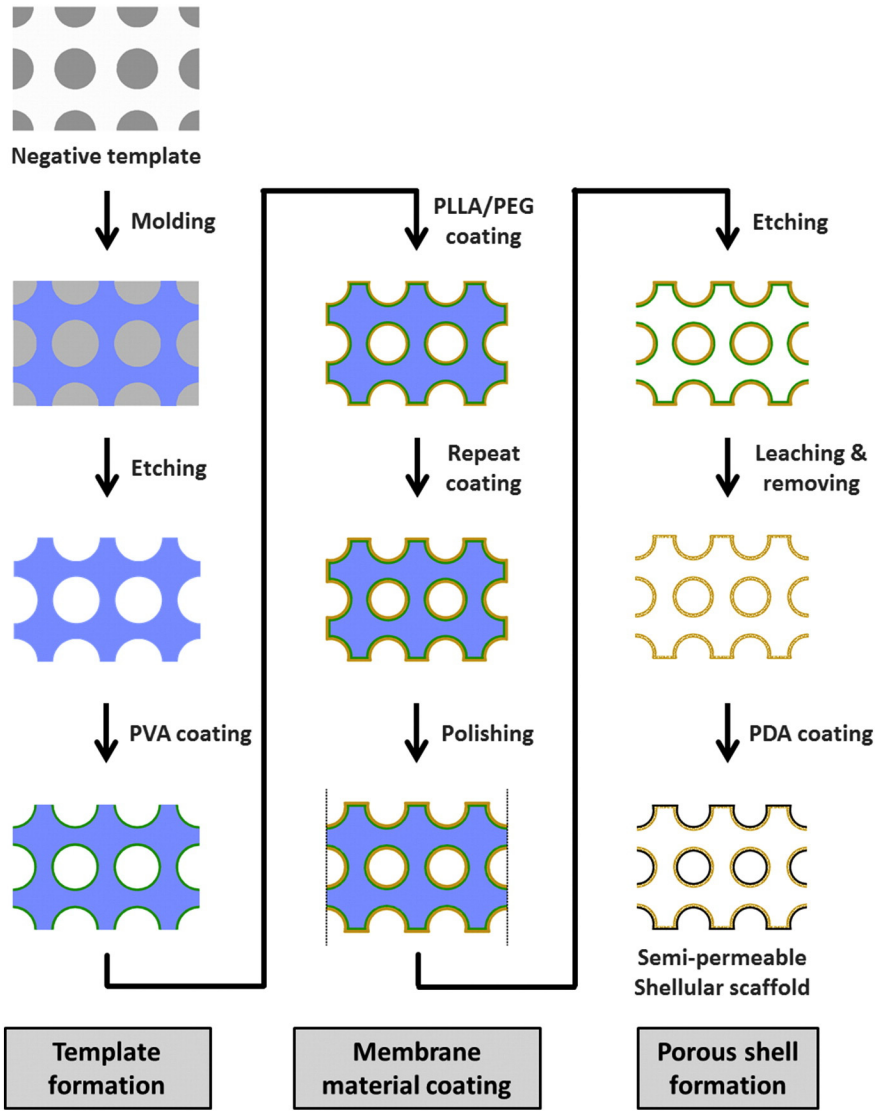

Fig. 2. Fabrication process of 3D membrane architecture specimens.

Another purpose of the heat treatment was to decrease the dissolution rate of the PLLA/PEG layer at contact with the solvent during subsequent dip-coatings. For Type-II and Type-III solutions, this process of dip-coating followed by heat-treatment was repeated until the thickness of the layer reached a desired value to provide sufficient strength and stiffness for the 3D membrane architecture, the final product. This is because when a thick layer was coated on the template through a single process, the coated solution was not uniformly distributed over the surface due to gravitation. However, coating and heat-treatment were conducted only once for the Type-I solution, because the biopolymer membrane formed by the solution was fast dissolving at contact with the solvent during subsequent dip-coatings even after the heat-treatment. Therefore, Type-I solution was not used for fabricating the specimens of 3D membrane architecture. It was only used to fabricate stand-alone membranes to see the microstructure.

2.2.4. Porous shell formation

After membrane material coating, two outermost surfaces of the biopolymer-coated template were mechanically polished to expose the substrate HMR template beneath the coated layer. The template was immersed in acetone to completely etch the HMR template and obtain a 3D membrane architecture consisting of PLLA/PEG membrane. The architecture was rinsed with DI water until acetone was completely removed. Afterwards, it was immersed in distilled water bath for approximately 4 h to leach out PEG porogen and remove the PVA top layer. Finally, the architecture was totally rinsed with DI water again to obtain the final product, i.e., 3D membrane architecture of porous PLLA.

In addition, to improve the hydrophilicity of its surface, polydopamine (PDA, another biopolymer) was coated on the 3D membrane architecture in a thickness of nano meter order [30]. For this purpose, 0.121 wt% of Tris-HCl aqueous solution was prepared first. Its pH level was then adjusted to approximately 8.5 by adding drops of HCl into the aqueous solution. Subsequently, DA was dissolved in Tris-HCl aqueous solution at concentration of 2 mg/ml for PDA coating. The 3D membrane architecture of porous PLLA was then immersed in this solution. After continuous stirring for 18 h, the porous PLLA architecture was rinsed several times with DI water to completely remove debris. Finally, the 3D membrane architecture, modified by PDA coating, was stored in 70% ethanol solution for sterilization.

2.3. Measurement of properties

2.3.1. Tensile test

Intrinsic tensile properties of the biopolymer membranes as constituent materials of the 3D membrane architecture were measured using a

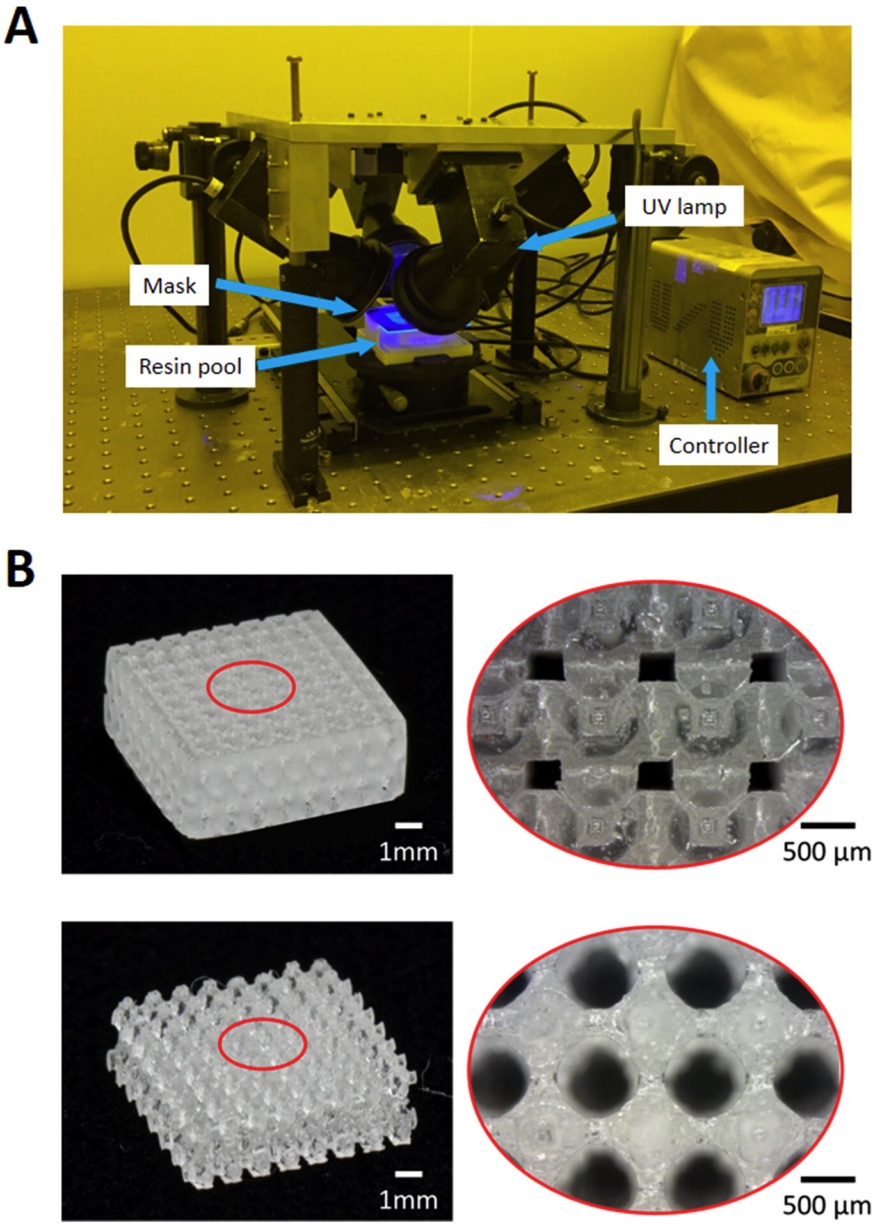

Fig. 3. (A) UV exposure system used for forming the negative template, (B) samples of the negative (top) and positive (bottom) templates with close-up top views.

home-made material tester. For this purpose, stand-alone membranes of the porous PLLA were prepared on glass slides through the exactly same process as that conducted on the positive HMR template, described above. In addition, membranes of non-porous PLLA were prepared to investigate the effect of porosity. After each membrane was cut into a long tape shape with length of 10 mm and width of 4 mm, its ends were bonded with two stainless steel foils using epoxy. Each specimen was installed between the upper and lower grips at the stainless steel foils. A miniature material tester used for tensile tests was driven by a step-motor actuator and a matching controller (Oriental Motors Co. and Suruga Seiki Co., Japan, respectively). Its displacement was controlled with 0.05 μm resolution at a rate of 1 mm/min. Because the membrane specimens were sufficiently compliant compared to the loading frame, displacement of the actuator monitored by the controller was assumed to be the same as that of the membrane specimen. Load cell was Lebow 3397-50 and test speed was set at 1 mm/min.

Table 1
Polymeric solute and organic solvent in biopolymer coating solutions.

Type	Polymers PLLA/PEG (wt%)	Solvent Chloroform/1,4-dioxane (vol%)
I	50/50	100/0
II	50/50	50/50
III	66.7/33.3	50/50

2.3.2. Compression test

Mechanical properties of the 3D membrane architecture under compressive loading were measured using an electro-hydraulic test system (INSTRON 8872) with a constant speed of 0.003 mm/s. Technical details are given in Han, et al. [21]. The overall dimensions of the 3D membrane specimens, which were also used in the permeability tests, were 5 mm * 5 mm * 2.85 mm. These 3D membrane specimens composed of non-porous PLLA and porous PLLA were tested in three different conditions (i.e., in dry condition for the samples of the non-porous PLLA and porous PLLA, and in wet condition for the samples of the porous PLLA). All specimens were modified by PDA coating. For tests in the wet condition,

scaffolds were pre-wetted with 70% ethanol for 2 h, and subsequently submerged in water before conducting compression test.

2.3.3. Wettability measurements

To estimate wettability of PLLA membrane, static water contact angles formed on the membranes were measured using a commercial drop shape analysis system (Phoenix 300, SEO Co., South Korea). Three types of the standalone membranes (nonporous PLLA membrane, porous PLLA membrane, and PDA-coated porous PLLA membrane) were cut into pieces of approximately 8 mm × 8 mm and pasted onto glass slides. Four samples were tested for each type. In addition, wettability tests were conducted for the 3D membrane architecture composed of the porous PLLA with or without PDA coating.

2.3.4. Permeability measurements

Permeability test of PDA-coated 3D membrane architecture was conducted at ambient condition. (A schematic of the test setup will be given later in this paper.) Top of the architecture was connected to a plastic tube using a UV cured Thiol-ene as glue. An end of the plastic tube was then hung on an edge of a small beaker before test. Aqueous BSA solution of 0.18 ml with a concentration of 2 mg/ml was injected into the internal sub-volume of the 3D membrane architecture, while aqueous PBS solution of 2 ml sub-volume was injected into the beaker. Thereafter, a sample of 0.1 ml was taken from the beaker every 0.5 h for 4 h. Variation in concentration of the BSA was measure with elapsed time using a UV–VIS spectrophotometer with a wavelength of 278 nm (Cary 300, Varian Inc., USA). Before the tests, calibration was conducted using five standard BSA solution samples.

3. Results and discussion

3.1. Properties of porous membranes

Microstructure of the standalone porous PLLA membranes prepared using the three types of the solutions (Table 1) was investigated by SEM. Typical SEM images are shown in Fig. 4A to I. Top views in the first column revealed porous surfaces, while cross-sectional views in the second column revealed sponge-like micro structures that were formed by leaching out the PEG phase. The third column shows the higher magnification images of the cross-sections. To get clearer images of the cross-sections, revealing the porosity and inter-connectivity, we broke the membrane specimens by pulling apart quickly after dipping into liquid nitrogen and obtained sharp cuts in the cross-sections. Fig. 4A to C are the images of the PLLA membrane that was prepared using the Type-I solution (with the single solvent). The least number of pores were observed on the surface, and cavities were less interconnected in the cross section than those prepared using the other types. In contrast, the rest images for Type-II and Type-III solutions (with the mixed solvent), i.e., Fig. 4D to F and Fig. 4G to I, respectively, revealed the more pores on the surfaces with the more interconnections among the cavities in the cross-sections. The rough surface morphology and higher porosity of membranes (Fig. 4D to I) prepared by the mixed solvent solutions were attributed to not only the leached-out PEG but also the small amount of crystallized PLLA from the blend solution [31]. Particularly, the microstructure of the membrane, that was prepared using the Type-III solution, was considerably fine and homogeneous. In addition, high concentration of PEG resulted in the highest porosity of 30 to 38% among these three membranes. Therefore, tensile test specimens and 3D membrane architecture specimens were prepared using only Type-

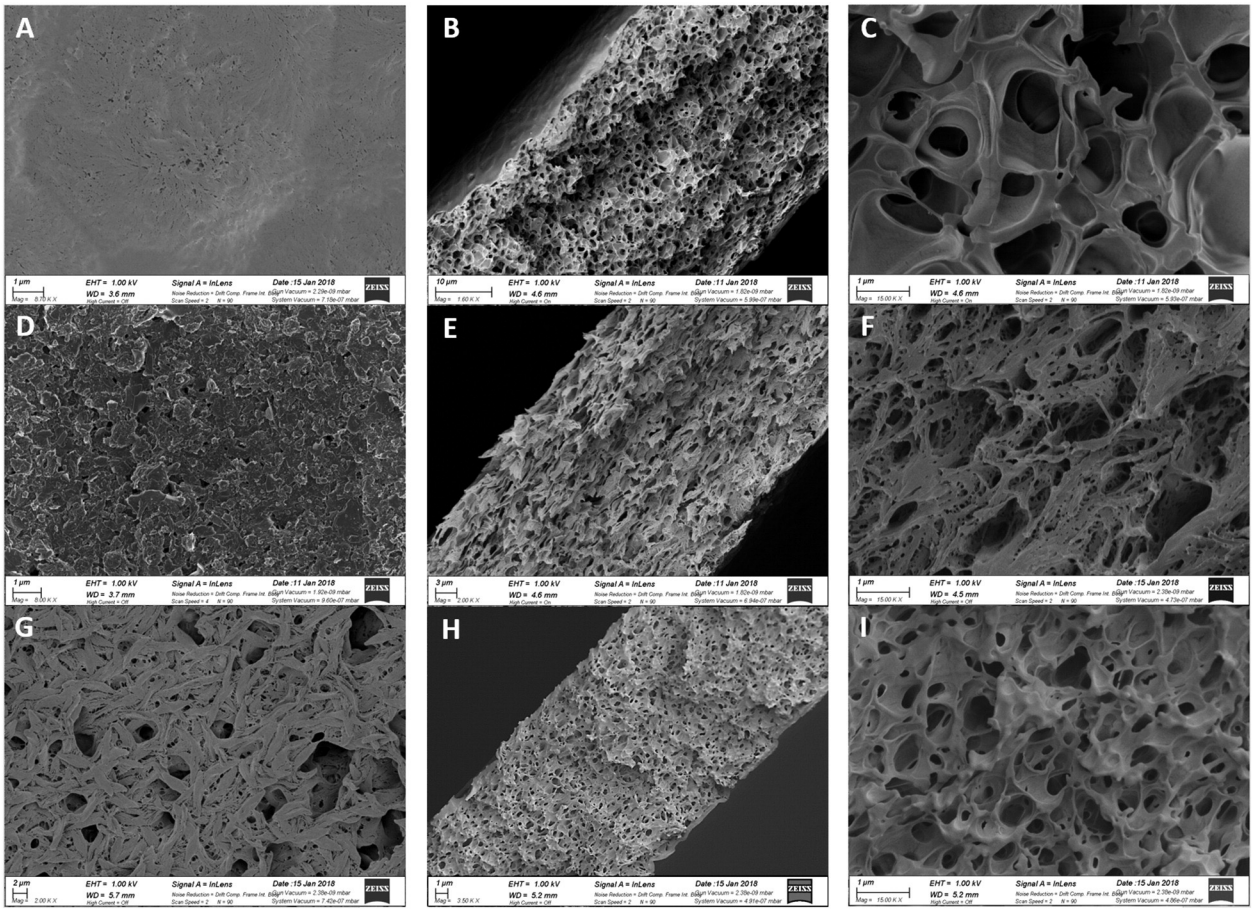

Fig. 4. SEM images of porous membranes, prepared using three different coating solutions: Type-I (A to C), Type-II (D to F), and Type-III (G to I).

III solution. The higher magnification images of the cross-sections, shown in the third column of the new SEM images, reveal that the average pore size of Type-I membrane is higher than those of Type-II and III membranes.

Fig. 5A shows a SEM image of a specimen of 3D membrane architecture. Note that the specimen was hollow and composed of a thin porous membrane. Also, to obtain its 3D geometry, a micro-CT image was obtained using an X-ray micro-tomography (Quantum GX, Perkin Elmer, Inc., USA). Fig. 5B shows the micro-CT image (red) of a specimen, overlapped with CAD image (grey) of *P*-surface, according to Eq. (4) with $k_1 = 0.3$, $k_2 = 1.4$, and volume fraction of $f = 0.44$. Despite some local errors, this figure revealed that the specimen had an overall configuration similar to the mathematical model of *P*-surface.

Fig. 5C and D show close-up SEM images for the 3D membrane architecture. These SEM images revealed smooth morphology with fine texture of the porous PLLA membrane achieved by leaching out the PEG porogen phase. When used as a tissue engineering scaffold, these pores had sizes of a few micrometers and were well interconnected to each other, which would allow the nutrients and metabolic wastes to pass through the shell membrane, while large-sized masses such as cells and extra-cellular matrix would remain. The membrane thickness of the specimens of 3D membrane architecture ranged from several micrometers to tens of micrometers depending on the number of repeated processes of coating and heat-treatment, as mentioned in the section of *membrane material coating*.

3.2. Mechanical properties

Fig. 6A compares tensile strengths of the nonporous PLLA membranes with those of the porous PLLA ones. The tensile strength of the nonporous membrane was 47.56 ± 1.74 MPa, while that of the porous membrane was 14.71 ± 0.92 MPa, which means that the strength was decreased to approximately one third due to the cavities in the membrane. Fig. 6B shows that the elongation of the nonporous membrane

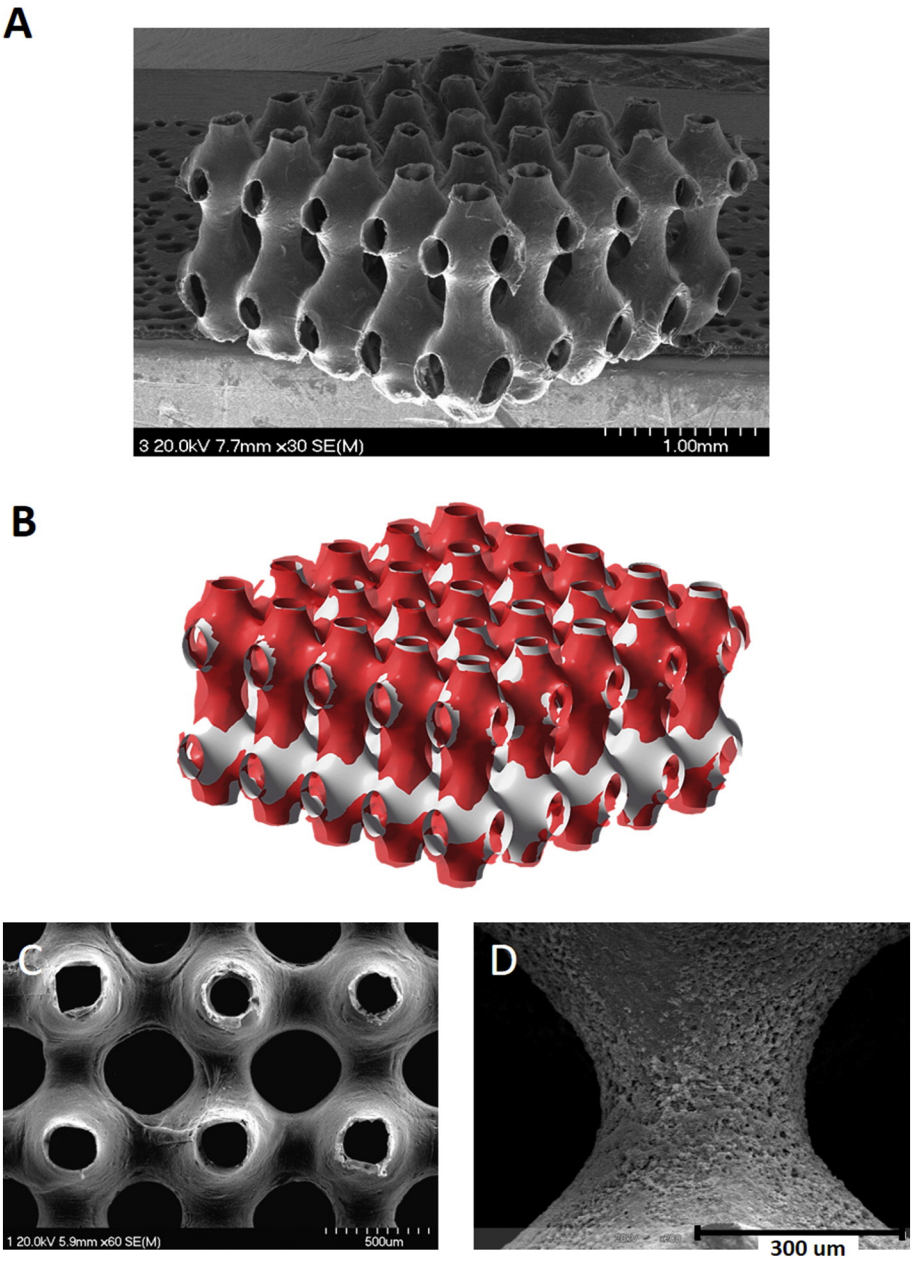

Fig. 5. (A) SEM image of a specimen of 3D membrane architecture, (B) Micro-CT image of the specimen, overlapped with the CAD image of the *P*-surface, according to Eq. (4), (C) and (D) close-up SEM images for the 3D membrane architecture.

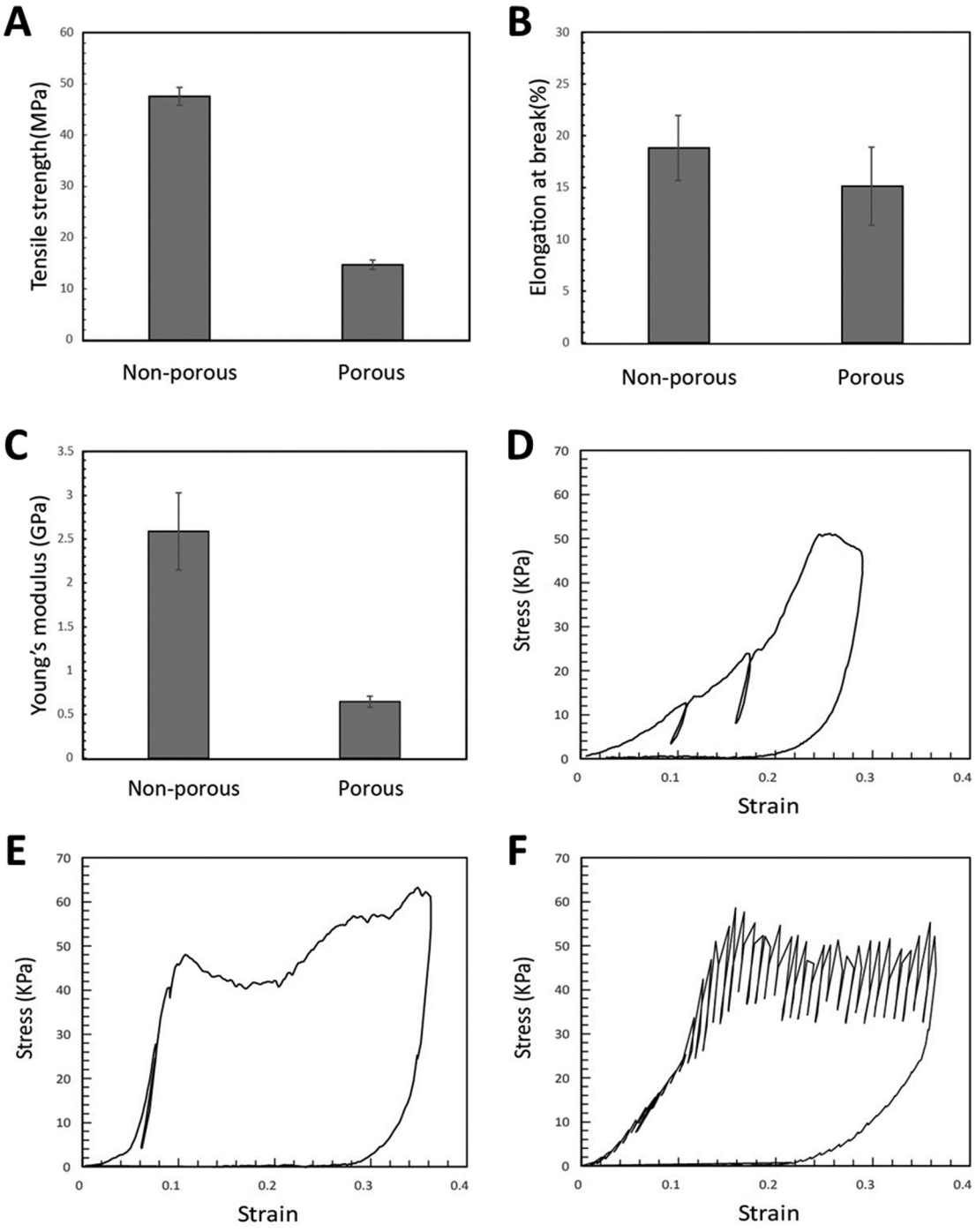

Fig. 6. (A) Tensile strengths, (B) elongation, and (C) Young's modulus of the nonporous PLLA and the porous PLLA membranes, (D), (E), and (F) stress-strain curves measured from the compression tests for the three types of 3D membrane architectures, i.e., the nonporous membrane architecture, porous membrane architectures in dry condition and wet condition, respectively.

was 18.83 ± 3.14%, while that of the porous membrane was 15.13 ± 3.77%. Unlike the strength, the elongation was only slightly decreased for the porous membrane.

Similar to the results of the tensile strength, the Young's modulus calculated from the slope of unloading segment in the stress strain curve was decreased from 2.59 ± 0.44 GPa for the nonporous membrane to 0.65 ± 0.06 GPa for the porous membrane due to the porosity to the membrane (Fig. 6C). The measured porosity of the porous membrane ranged from 30 to 38%. Considering the membrane porosity, the decrease in the tensile strength and Young's modulus was reasonable. An independent test with a specimen without the PDA coating revealed that the nano-scale thickness of PDA coating had virtually no influence on the strength of membrane.

Fig. 6D, E, and F show the stress-strain curves measured from the compression tests for the three types of 3D membrane architectures, i.e., the nonporous membrane architecture, porous membrane architecture in dry condition, and porous membrane architecture in wet condition, respectively. Densities of these three specimens that were measured from the overall volumes and the weights were 0.0282, 0.0388, and 0.0442 g/cm^3, respectively, at dry state. Their peak strengths were 51.02, 47.66, and 40.88 kPa, respectively. These results revealed that the strength became lower in wet condition. The

nonporous membrane architecture had the highest the strength despite its lowest density. However, compared with the tensile strengths, shown in Fig. 6A, the compressive strength of the nonporous membrane architecture was not much higher than that of the porous one. Also, the overall slope of the stress strain curve at the loading phase for the nonporous membrane architecture, shown in Fig. 6D, was very low compared to those for the porous membrane architecture. The low compressive strength and low stiffness of the nonporous membrane architecture were attributed to the thin wall (about 5 μm), composing the architecture. Namely, the thin-walled architecture easily buckled and collapsed under compressive loading. In contrast, the relatively thicker wall of the porous membrane architecture (about 15 μm) provided much higher stiffness even at a similar density. This result justifies the use of the porous membrane as constituent material for the 3D membrane architecture even in terms of the mechanical properties.

The stress-strain curve, shown in Fig. 6F, was measured from the 3D membrane architecture in wet condition and revealed an unusual pattern comprising lots of unloading line segments. The mechanism and the consequent effect on the tissue engineering function will be explored in near future.

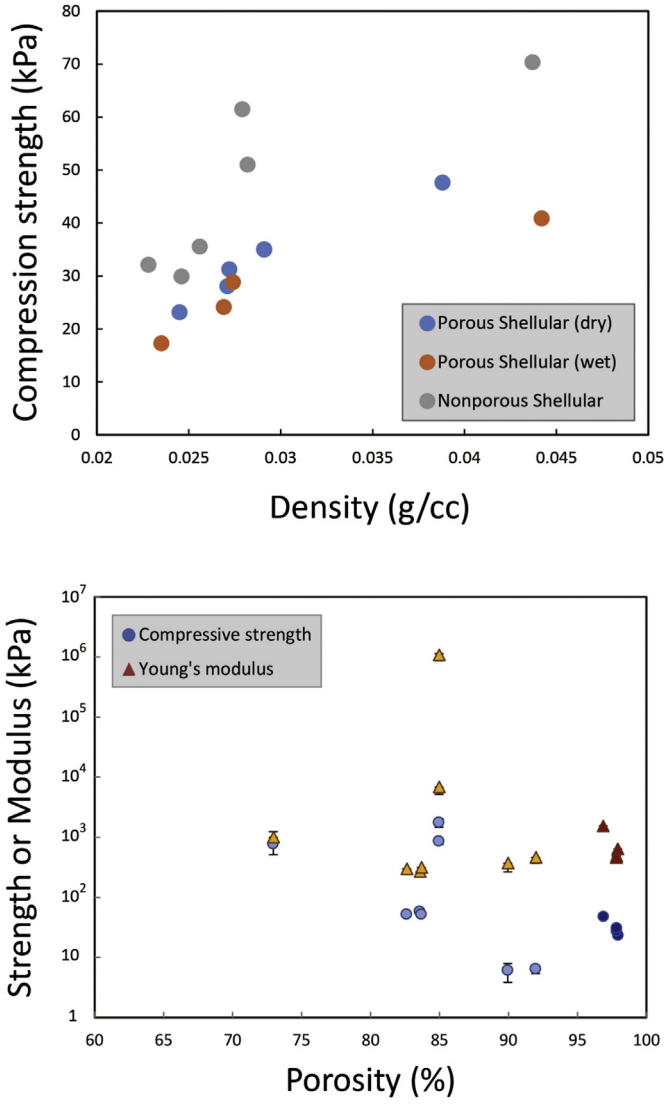

Fig. 7. (A) Variation of the compressive strength of the three membrane architectures according to the overall density (the weight per the overall volume) in a range from 0.02 to 0.05 g/cm^3, (B) strengths and Young's moduli of our 3D membrane architectures depending on the porosities, in comparison with the previous typical scaffolds.

Fig. 7A summarizes variation in the compressive strength of the three membrane architectures according to the overall density (weight per overall volume) ranging from 0.02 to 0.05 g/cm^3. Despite large scatter, it was clear that the strength of non-porous membrane architecture was always higher than those of the porous membrane architectures for a given density. The difference was increased as the density was increased (i.e., the membrane thickness was increased). The strengths of the porous membrane architectures in wet condition were not much lower than those in dry condition.

Fig. 7B summarizes the compress strengths and Young's moduli of the 3D membrane architecture depending on the porosities in comparison with previous typical scaffolds, chosen in this study. All these scaffolds were developed for regeneration of bones or cartilages using five different constituent materials: HA (Hydroxyapatite), PDLLA (poly (D,L-lactic acid)) [32], PU (Polyurethane) [33], cellulose/chitosan [34], and PLG (poly (L-lactide-*co*-glycolide)) [35]. The most notable detail observed in this figure was the high overall porosities of our 3D membrane architecture (denoted by the red and dark blue colored symbols), ranging from 96.9% to 98.1%. Such high porosities, compared to the previous scaffolds, were attributed to the porous and thin membranes composing these 3D membrane architectures. Despite of their high porosity, the strengths and Young's moduli of our 3D membrane architectures were comparable to those of the PLG scaffolds with porosities of approximately 83% [35]. They were higher than those of cellulose/chitosan scaffolds with porosities of approximately 91% [34]. These results demonstrate their superior mechanical properties of our 3D membrane architectures even with high porosities.

3.3. Surface wettability

Wettability of a biomaterial surface plays a critical role in cell adhesion, migration, and proliferation. As a synthetic biopolymer, PLLA is intrinsically hydrophobic. To investigate the influence of surface modification, water contact angles (WCA) were measured for the pristine surfaces or the surface modified by PDA. Fig. 8A shows the WCA data measured from the flat surfaces of the non-porous, porous, and PDA-coated standalone membranes. The WCA of the nonporous PLLA membrane was observed 71.52° ± 4.19°, while that of the porous PLLA membrane was 110.88° ± 10.70°, that is, more hydrophobic. However, after coating with PDA, the WCA of the porous PLLA membrane was decreased to 58.51° ± 3.50°, indicating much improved hydrophilicity of the surface. See the shapes of the water drops on the membranes in Fig. 8A. Interestingly, without coating with PDA, the 3D membrane architecture of porous PLLA was so hydrophobic that the water droplet formed on its top (Fig. 8B). However, after coating with PDA, the water droplet was instantaneously absorbed into the membrane architecture (Fig. 8C), demonstrating a dramatic effect of the PDA-coating on surface.

3.4. Protein permeability

Fig. 8D is a schematic of the permeability test setup. Fig. 8E shows variation of concentration of the BSA in the beaker measured with the elapsed time. Because the porous membrane of the 3D architecture was designed to allow nutrient and oxygen to pass through it, the variation in concentration of the BSA in the beaker represented the permeability of the porous PLLA membrane. This figure shows that it took about 3 h for the concentration of BSA in the beaker to converge to the same level as that in the internal sub-volume. The rate may be changeable depending on the blending method, blend ratio of PLLA and PEG, and even ambient temperature. Therefore, the condition of the blending needs to be determined for a specific permeability.

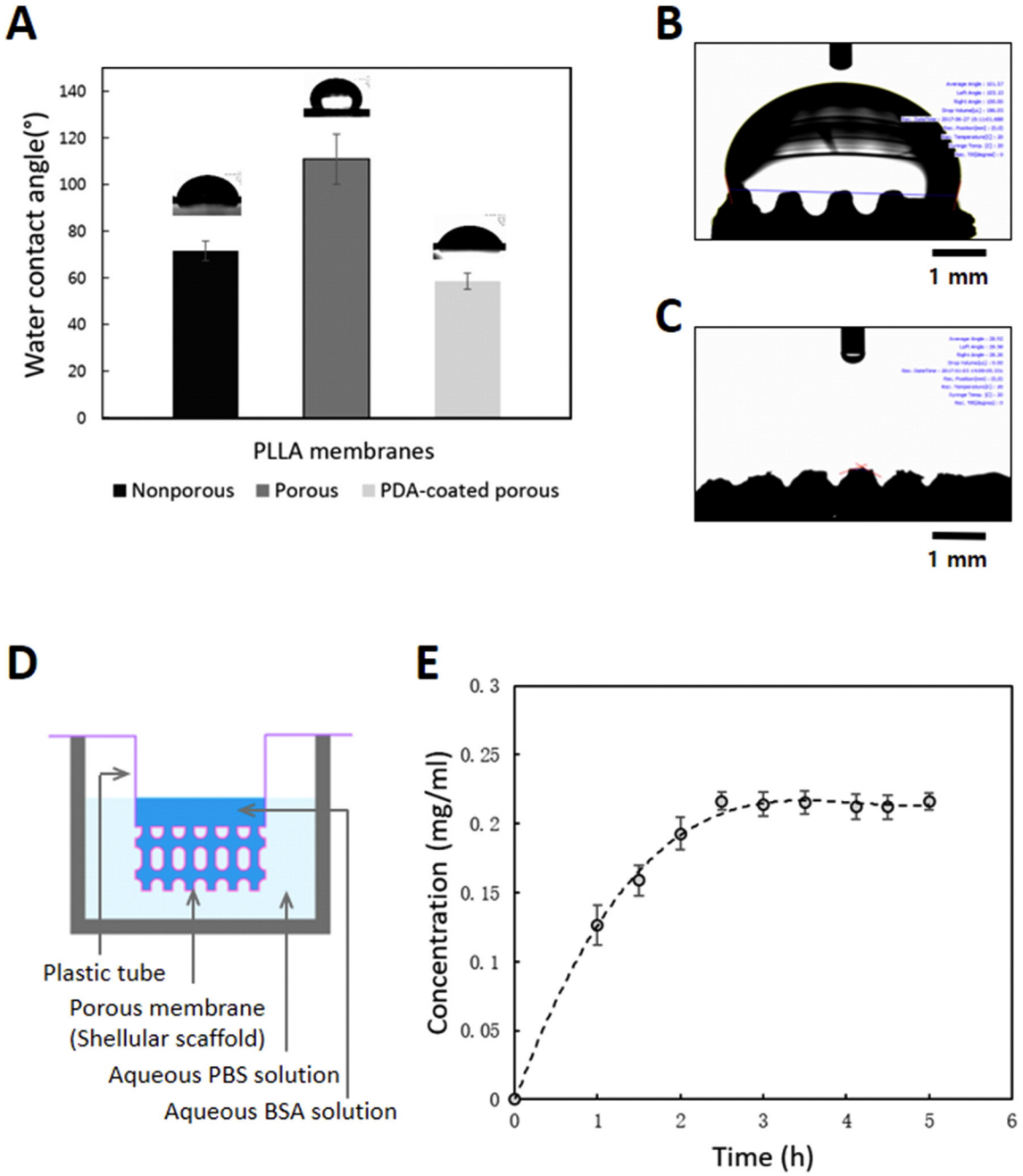

Fig. 8. (A) water contact angles (WCA) measured from the flat surfaces of the non-porous, porous, and PDA-coated standalone membranes, (B) and (C) photos of the water droplet formed on the top of the pristine specimen of 3D membrane architectures and no water droplet on the top of the PDA-coated specimen, respectively, (D) a schematic of the permeability test setup and (E) variation of concentration of the BSA in the beaker measured with the elapsed time.

4. Concluding remarks

This study introduced a novel design of tissue engineering scaffold without clogging issues from growing cells. The novel design of 3D membrane architecture was composed of a single semi-permeable polymer membrane in a TPMS configuration with two non-intersecting void sub-volumes. One sub-volume was used for cell culture, while the other served as a perfusion channel. Mass transfer between cells and perfusion channel is implemented through the interfacial semipermeable membrane. As a preliminary study of such Shellular scaffold, this paper described the fabrication process of this 3D membrane architecture, based on 3D UV photo-lithography and porogen leaching technique. In addition, its mechanical properties, microstructure, wettability, and permeability were evaluated. Conclusions are as follows:

i). Proper blend of coating solution was determined to obtain the biopolymer PLLA porous membrane with porosity of 30 to 38% for the 3D membrane architecture.
ii). The fabrication technique provided *P*-surface-like architecture composed of a porous membrane with smooth and fine texture, yielding very low overall density, ranging from 0.02 to 0.05 g/cm^3 (i.e., high porosity of approximately 97%).
iii). Despite their high porosity, these 3D membrane architectures had strengths and Young's moduli, comparable to

those of PLG scaffolds and Cellulose/chitosan scaffolds that were developed for regeneration of bones or cartilages.

iv). Wettability, scaled by hydrophilicity, of the PDA-coated PLLA porous membrane was sufficiently high, resulting in instant absorption of water droplet into the scaffold.

v). Permeability of the porous PLLA membrane was sufficiently high so as to allow BSA to pass through it, and its concentration was homogenized in about 3 h. The rate may be changeable depending on blending method, blend ratio of PLLA and PEG, and ambient temperature. The condition of the blending needs to be determined for a specific permeability.

The high porosity of such 3D membrane architecture is expected to be degraded and absorbed without causing any harm. Additional studies including in-vitro engineering of living tissues are being conducted using chondrocyte cells in our research group to examine the feasibility of this intriguing scaffold that is integrated with an independent vascular system (i.e., mass transfer channel) and continuously provides nutrients and oxygen supply to proliferating cells as well as removal of waste by the thin semi-permeable membrane. The results will be reported in the near future.

Acknowledgements

This research was supported by Basic Science Research Program through the National Research Foundation of Korea (NRF) funded by the Ministry of Science, ICT and Future Planning (No.2015R1A2A1A01003702). The authors thank Y.C. Jung for help to draw CAD images and take micro-CT images.

References

[1] H. Mehdizadeh, S.I. Somo, E.S. Bayrak, E.M. Brey, A. Cinar, Design of polymer scaffolds for tissue engineering applications, Ind. Eng. Chem. Res. 54 (2015) 2317–2328.
[2] F. Khan, M. Tanaka, S.R. Ahmad, Fabrication of polymeric biomaterials: a strategy for tissue engineering and medical devices, J. Mater. Chem. 3 (2015) 8224–8249.
[3] I. Martin, D. Wendt, M. Heberer, The role of bioreactors in tissue engineering, Trends Biotechnol. 22 (2004) 80–86.
[4] L.E. Freed, G. Vunjak-Novakovic, Culture of organized cell communities, Adv. Drug Deliv. Rev. 33 (1998) 15–30.
[5] S. Hyde, Z. Blum, T. Landh, S. Lidin, B.W. Ninham, S. Andersson, K. Larsson, The Language of Shape, Elsevier, 1996.
[6] F.P.W. Melchels, A.M.C. Barradas, C.A. van Blitterswijk, J. de Boer, J. Feijen, D.W. Grijpma, Effects of the architecture of tissue engineering scaffolds on cell seeding and culturing, Acta Biomater. 6 (2010) 4208–4217.
[7] S. Rajagopalan, R.A. Robb, Schwarz meets Schwann: design and fabrication of biomorphic and durataxic tissue engineering scaffolds, Med. Image Anal. 10 (2006) 693–712.
[8] S.C. Kapfer, S.T. Hyde, K. Mecke, C.H. Arns, G.E. Schröder-Turk, Minimal surface scaffold designs for tissue engineering, Biomaterials 32 (2011) 6875–6882.
[9] H. Montazerian, E. Davoodi, M. Asadi-Eydivand, J. Kadkhodapour, M. Solati-Hashjin, Porous scaffold internal architecture design based on minimal surfaces: a compromise between permeability and elastic properties, Mater. Des. 126 (2017) 98–114.
[10] A. Ataee, Y. Li, D. Fraser, G. Song, C. Wen, Anisotropic Ti-6Al-4V gyroid scaffolds manufactured by electron beam melting (EBM) for bone implant applications, Mater. Des. 137 (2018) 345–354.
[11] A. Yánez, A. Cuadrado, O. Martel, H. Afonso, D. Monopoli, Gyroid porous titanium structures: a versatile solution to be used as scaffolds in bone defect reconstruction, Mater. Des. 140 (2018) 21–29.
[12] S.M. Giannitelli, D. Accoto, M. Trombetta, A. Rainer, Current trends in the design of scaffolds for computer-aided tissue engineering, Acta Biomater. 10 (2014) 580–594.
[13] F.P.W. Melchels, K. Bertoldi, R. Gabbrielli, A.H. Velders, J. Feijen, D.W. Grijpma, Mathematically defined tissue engineering scaffold architectures prepared by stereolithography, Biomaterials 31 (2010) 6909–6916.
[14] J. Visser, F.P.W. Melchels, J.E. Jeon, E.M. van Bussel, L.S. Kimpton, H.M. Byrne, W.J.A. Dhert, P.D. Dalton, D.W. Hutmacher, J. Malda, Reinforcement of hydrogels using three-dimensionally printed microfibers, Nat. Commun. 6 (2015) 6933.
[15] D. Loessner, C. Meinert, E. Kaemmerer, L.C. Martine, K. Yue, P.A. Levett, T.J. Klein, F.P.W. Melchels, A. Khademhosseini, D.W. Hutmacher, Functionalization, preparation and use of cell-laden gelatin methacryloyl–based hydrogels as modular tissue culture platforms, Nat. Protoc. 11 (2016) 727–746.
[16] B.J. Klotz, D. Gawlitta, A.J.W.P. Rosenberg, J. Malda, F.P.W. Melchels, Gelatin-methacryloyl hydrogels: towards biofabrication-based tissue repair, Trends Biotechnol. 34 (2016) 394–407.
[17] F.P.W. Melchels, M.M. Blokzijl, R. Levato, Q.C. Peiffer, M. De Ruijter, W.E. Hennink, T. Vermonden, J. Malda, Hydrogel-based reinforcement of 3D bioprinted constructs, Biofabrication 8 (2016), 035004.
[18] M.T. Poldervaart, B. Goversen, M. de Ruijter, A. Abbadessa, F.P.W. Melchels, F.C. Öner, W.J.A. Dhert, T. Vermonden, J. Alblas, 3D bioprinting of methacrylated hyaluronic acid (MeHA) hydrogel with intrinsic osteogenicity, PLoS One 12 (2017), e0177628.
[19] M. Lovett, K. Lee, A. Edwards, D.L. Kaplan, Vascularization strategies for tissue engineering, Tissue Eng. B Rev. 15 (2009) 353–370.
[20] N.M.S. Bettahalli, Membrane Supported Scaffold Architectures for Tissue Engineering(PhD Thesis) University of Twente, Enschede, The Netherlands, 2011.
[21] S.C. Han, J.W. Lee, K.J. Kang, A new type of low density material: shellular, Adv. Mater. 27 (2015) 5506–5511.
[22] M.G. Lee, J.W. Lee, S.C. Han, K. Kang, Mechanical analyses of "shellular", an ultralow-density cellular metal, Acta Mater. 103 (2016) 595–607.
[23] B.D. Nguyen, J.S. Cho, K. Kang, Optimal design of "shellular", a micro-architectured material with ultralow density, Mater. Des. 95 (2016) 490–500.
[24] B.D. Nguyen, Y.C. Jeong, K. Kang, Design of the P-surfaced shellular, an ultra-low density material with micro-architecture, Comput. Mater. Sci. 139 (2017) 162–178.
[25] N.A. Fleck, V.S. Deshpande, M.F. Ashby, Micro-architectured materials: past, present and future, Proc. R. Soc. London, Ser. A 466 (2010) 2495–2516.
[26] T. Femmer, A.J.C. Kuehne, J. Torres-Rendon, A. Walther, M. Wessling, Print your membrane: rapid prototyping of complex 3D-PDMS membranes via a sacrificial resist, J. Membr. Sci. 478 (2015) 12–18.
[27] Q.L. Loh, C. Choong, Three-dimensional scaffolds for tissue engineering applications: role of porosity and pore size, Tissue Eng. B Rev. 19 (2013) 485–502.
[28] A.J. Jacobsen, W. Barvosa-Carter, S. Nutt, Micro-scale truss structures formed from self-propagating photopolymer waveguides, Adv. Mater. 19 (2007) 3892–3896.
[29] S. Selvam, W.V. Chang, S.C. Yiu, Microporous poly(L-lactic acid) membranes fabricated by polyethylene glycol solvent-cast/particulate leaching technique, Tissue Eng. Part C Methods 15 (2009) 463–474.
[30] S.S. Huang, N.Y. Liang, Y. Hu, X. Zhou, N. Abidi, Polydopamine-assisted surface modification for bone biosubstitutes, Biomed. Res. Int. 2016 (2016), 2389895.
[31] E. Rezabeigi, P.M. Wood-Adams, R.A.L. Drew, Production of porous polylactic acid monoliths via nonsolvent induced phase separation, Polymer 55 (2014) 6743–6753.
[32] M.M.C.G. Silva, L.A. Cyster, J.J.A. Barry, X.B. Yang, R.O.C. Oreffo, D.M. Grant, C.A. Scotchford, S.M. Howdle, K.M. Shakesheff, F.R.A.J. Rose, The effect of anisotropic architecture on cell and tissue infiltration into tissue engineering scaffolds, Biomaterials 27 (2006) 5909–5917.
[33] A. Asefnejad, M.T. Khorasani, A. Behnamghader, B. Farsadzadeh, S. Bonakdar, Manufacturing of biodegradable polyurethane scaffolds based on polycaprolactone using a phase separation method: physical properties and in vitro assay, Int. J. Nanomedicine 6 (2011) 2375–2384.
[34] T.T. Nge, M. Nogi, H. Yano, J. Sugiyama, Microstructure and mechanical properties of bacterial cellulose/chitosan porous scaffold, Cellulose 17 (2010) 349–363.
[35] E. Pamula, E. Filova, L. Bacakova, V. Lisa, D. Adamczyk, Resorbable polymeric scaffolds for bone tissue engineering: the influence of their microstructure on the growth of human osteoblast-like MG 63 cells, J. Biomed. Mater. Res. A 89 (2009) 432–443.